An Effective Modification of Conventional Beamforming Methods Suitable for Realistic Linear Antenna Arrays

Zaharias D. Zaharis, *Senior Member, IEEE*, Ioannis P. Gravas, *Student Member, IEEE*, Pavlos I. Lazaridis, *Senior Member, IEEE*, Traianos V. Yioultsis, *Member, IEEE*, Christos S. Antonopoulos, *Senior Member, IEEE*, and Thomas D. Xenos

***Abstract*— Antenna array beamforming (BF) refers to a real-time procedure that aims at calculating the proper feeding weights applied to the array elements in order to create a main lobe and a number of nulls toward respective preassigned directions. Most of the research performed on BF has been based on a simplified mathematical model, which ignores the nonisotropic radiation pattern of the array elements and the element mutual coupling. This article introduces an innovative way to incorporate the actual radiation pattern of the array elements and the element coupling into two popular deterministic BF methods, thus making these methods applicable to realistic antenna arrays. These two modified methods are applied in several scenarios, where a desired signal and several interference signals with various directions of arrival are received by a realistic microstrip linear antenna array. The statistical analysis performed in every scenario demonstrates the validity and effectiveness of the proposed modification.**

***Index Terms*— Antenna array beamforming (BF), direction of arrival (DoA), microstrip arrays, minimum variance distortionless response (MVDR), mutual coupling, null steering beamforming (NSB).**

I. Introduction

ANTENNA array beamforming (BF) is related to a particular problem that has to be solved in real time. It concerns the calculation of feeding weights applied by a proper feeding network to the elements of the antenna array in order to make the array create a main lobe and a number of radiation nulls toward respective preassigned directions [1]–[19]. In fact, the main lobe direction must coincide with the direction of arrival (DoA) of a desired incoming signal (DIS), while the directions of the nulls must coincide with DoAs of the respective undesired incoming signals (UISs). Usually, a UIS is an interference signal received by the antenna array at the same time as DIS. Therefore, the null creation helps the array to suppress every UIS and ameliorate the reception of DIS, thus improving the signal-to-interference-plus-noise ratio (SINR).

The great difficulty in solving this problem is that the feeding weights must be calculated again and again in real time and every time when changes occur in DoA of a DIS or in DoA of a UIS. In such ever-changing environments, evolutionary optimization methods [20]–[28] are not practically useful, because they need much time to give a solution due to their iterative structure. Of course, there is always the option of using neural networks (NNs) [29]–[32], which are capable of keeping the performance of a beamformer at sufficient levels, while providing an instant response. In fact, the efficiency of the NNs is due to the use of the data derived from deterministic or evolutionary methods. These data are used for NN training, which takes place before the NNs come into operation. By applying training as a preliminary process, an NN improves its efficiency and due to its structure it also provides immediate response. Nevertheless, the NN training is a time-consuming process, not to mention the time required if an evolutionary method is employed to extract all these training data. In addition, the training process may ensure the efficiency and functionality of an NN only in stable electromagnetic environments. Changes in DoA of a DIS or in DoA of a UIS create an ever-changing environment, which means that new training data must continuously be extracted and an NN training process utilizing these new data must continuously be performed, thereby converting these two time-consuming processes (data extraction and NN training) into real-time processes. Thus, it becomes evident that time response and efficiency of NN are two conflicting issues in such an environment.

On the other hand, deterministic methods are mostly suitable, because the absence (or the small number) of iterations and the lack of need for training provide incredibly fast solution to the problem, and for this reason several such methods have been proposed so far [4]–[19]. Nevertheless, most of the research performed so far on deterministic methods of antenna array BF has been based on a simplified

Manuscript received October 16, 2019; revised February 9, 2020; accepted February 13, 2020. Date of publication March 13, 2020; date of current version July 7, 2020. This work was supported by Greece and the European Union [European Social Fund (ESF)] through the Operational Program "Human Resources Development, Education and Lifelong Learning" in the context of the project "Strengthening Human Resources Research Potential via Doctorate Research" implemented by the State Scholarships Foundation (IKY) under Grant MIS-5000432. *(Corresponding author: Zaharias D. Zaharis.)*

Zaharias D. Zaharis, Ioannis P. Gravas, Traianos V. Yioultsis, Christos S. Antonopoulos, and Thomas D. Xenos are with the Department of Electrical and Computer Engineering, Aristotle University of Thessaloniki, 54124 Thessaloniki, Greece (e-mail: zaharis@auth.gr; igravas@auth.gr; traianos@auth.gr; chanto@auth.gr; tdxenos@auth.gr).

Pavlos I. Lazaridis is with the Department of Engineering and Technology, University of Huddersfield, Huddersfield HD1 3DH, U.K. (e-mail: p.lazaridis@hud.ac.uk).

Color versions of one or more of the figures in this article are available online at http://ieeexplore.ieee.org.

Digital Object Identifier 10.1109/TAP.2020.2977822

mathematical model, because the antenna array factor is treated as the total radiation pattern, without taking into account the particular nonisotropic radiation pattern that the array elements may produce and without considering the mutual coupling between the array elements.

This article introduces a novel idea to incorporate the actual nonisotropic radiation pattern produced by the array elements and the mutual coupling between these elements into deterministic BF methods, thus making these methods applicable to realistic antenna arrays. Two popular BF methods, namely the minimum variance distortionless response (MVDR) method and the null steering BF (NSB) method [1], [2], are properly modified according to this new idea in order to be applied on a realistic microstrip linear antenna array. To the best of the authors' knowledge, such a modification has never been applied to BF methods.

The validity and the effectiveness of the proposed modification are thoroughly examined in Section VI, by implementing several scenarios of signal reception and by applying a detailed statistical analysis in every scenario. The results prove that the proposed modification makes the BF methods capable of responding accurately, despite the nonisotropic radiation pattern of the array elements and the mutual coupling between these elements.

II. Prior Art

A lot of research related to BF can be found in the literature. A big part of this research concerns deterministic BF methods [4]–[19]. The numerical pattern synthesis technique, proposed in [4], can be used for BF and, due to its iterative structure, it can additionally be employed for sidelobe level (SLL) control. A combination of BF and multiple-input multiple-output (MIMO) techniques is studied in [5] and [6]. Efficient broadcasting through joint network coding and BF is proposed in [7], while BF is employed in [8] to implement virtual MIMO broadcasting. An interesting comparison between analog and digital BF is performed in [9]. Adaptive BF methods are proposed in [10] and [11], while an MVDR beamformer for null level control via quadratic programming is proposed in [12]. BF methods with sidelobe suppression are proposed in [13]–[16], while optimal BF methods implemented through convex optimization are proposed in [17] and [18]. Finally, the method proposed in [19] for pattern synthesis with low SLL takes into account the mutual coupling between the elements of a linear antenna array and could potentially be used to perform BF. All the methods proposed in these literature seem to be really innovative. However, they deal with the BF problem from a theoretical aspect because, unlike the modified BF methods proposed in this article, they ignore the nonisotropic radiation pattern of the array elements and the element mutual coupling. The only exception is the pattern synthesis method proposed in [19]. However, the iterative fast Fourier transform (FFT) algorithm employed in this method may induce a time response issue if the method is used to perform BF in a rapidly changing environment.

Another part of the research related to BF concerns evolutionary optimization methods [20]–[28]. A BF method is proposed in [20] by using an evolutionary method called invasive weed optimization (IWO). A binary version of particle swarm optimization (PSO), which applies mutation to the velocities of the particles, is proposed in [21] to implement a BF method, while a differential evolution algorithm is employed for BF in [22]. Various evolutionary methods, such as PSO in [23], IWO in [24], and genetic algorithms in [25], are employed to perform BF and also to achieve a low SLL. A hybrid method that integrates interval analysis and PSO is applied in [26] and [27] to implement BF in linear antenna arrays. Finally, a combination of the ant colony optimization and the least mean squares algorithm is proposed in [28] to perform BF and also to achieve a low SLL in thinned fractal antenna arrays. All these evolutionary methods are really effective in a stable or slowly changing electromagnetic environment. Nevertheless, they may become ineffective in fast-changing environments, because they need a considerable amount of time to give a solution due to their iterative structure, as mentioned in Section I. It is therefore apparent that a real-time process, such as the BF, requires primarily noniterative algorithms, because such algorithms usually have instant response, as is the case with the modified BF methods proposed in this article.

NNs have also been used for BF [29]–[32]. In [29] and [30], three-layer radial basis function NNs trained by data derived from deterministic BF methods are employed for BF. In [31] and [32], four-layer feed-forward NNs trained by data derived from evolutionary methods (i.e., a binary PSO variant in [31] and an IWO variant in [32]) are employed to perform BF and also to achieve a low SLL. As explicitly explained in Section I, an NN has the ability to work efficiently only after the accomplishment of two time-consuming processes, that is, the extraction of training data and the NN training. It is evident that time-consuming processes can be implemented only in stable or slowly changing electromagnetic environments. In an ever-changing environment where states change rapidly, these two processes (data extraction and NN training) usually fail to complete before every subsequent state change, thus resulting in NN's inability to work efficiently. Therefore, the modified BF methods proposed here are preferable, because no training process is required prior to their usage.

In addition, a lot of applications related to BF can be found in the literature [17], [18], [33]–[42]. Optimal BF methods suitable for airborne radars are proposed in [17] and [18], while in [33] an intelligent BF system is proposed for the reception of direct broadcast satellite signals. A monolithic integration of a modified Butler matrix BF network and a four-arm spiral antenna is implemented in [34] for efficient operation from 50 to 75 GHz. A BF system is proposed in [35] for the reception of digital video broadcasting second generation terrestrial signals in high-speed train environments. A linearly constrained minimum variance BF method is presented in [36] as a technique to improve the calibration efficiency of an array-fed reflector antenna. In [37], various BF strategies that utilize the available excitation modes are applied to a quad-mode antenna in order to maximize the gain, the signal-to-noise ratio (SNR), and the polarization discrimination, while maintaining a minimum noise over the field of view. In [38], efficient BF solutions are proposed to

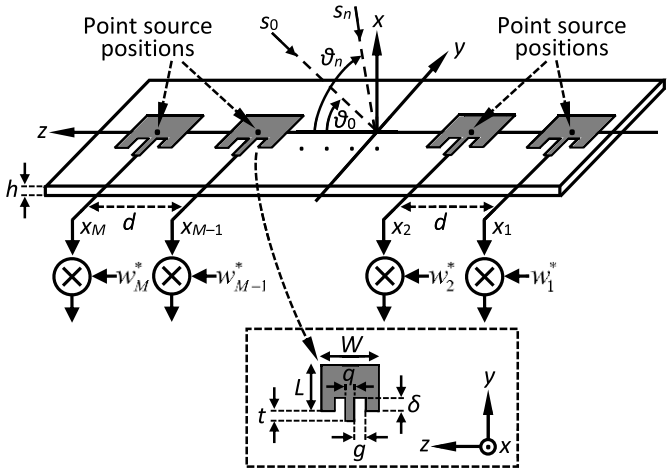

Fig. 1. Microstrip linear array used in receiving mode by a beamformer.

improve the quality of service in the 60 GHz band covered by the IEEE 802.11ad wireless networking standard. An optimal BF algorithm, suitable for antenna arrays used in future multibeam radiometers, is introduced and evaluated in [39], while novel digital BF array feeds are proposed in [40] to improve the performance of the microwave radiometers used in future ocean observation missions. In [41], a holistic design procedure together with a dedicated optimal BF process has been developed for the next generation multibeam radiometer systems. Finally, a novel reconfigurable antenna, operating from 3.5 to 5.5 GHz, is proposed in [42] for beam-steering, which is achieved by a proper control of p-i-n diodes. The BF methods proposed here have properly been modified in order to be applicable to realistic antenna arrays. Consequently, these methods are expected to be utilized in a considerable number of real-life applications related to BF.

III. Conventional BF Methods

According to the theoretical aspect of the BF problem, a DIS s_0 and N UISs s_n $(n = 1, \ldots, N)$ are received at frequency f (that corresponds to wavelength λ) by a linear array of M ideal point sources $(M > N)$ [1], [2]. The DoA of every signal s_n $(n = 0, 1, \ldots, N)$ is defined by a respective polar angle θ_n $(n = 0, 1, \ldots, N)$, which actually is the angle between DoA of the signal and the z-axis (see Fig. 1) and therefore it can be called as "angle of arrival" (AoA). The point sources are arranged along the z-axis and are uniformly spaced at distance d. It is easy to realize that each source produces an omnidirectional radiation pattern and that no coupling exists between any two sources. The radiation pattern of such an array is expressed by the antenna array factor as follows:

$$AF(\theta) = \sum_{m=1}^{M} I_m \exp(j\beta z_m \cos\theta) \tag{1}$$

where I_m $(m = 1, \ldots, M)$ are the currents applied to the point sources, β is the free space wavenumber $(\beta = 2\pi/\lambda)$, z_m $(m = 1, \ldots, M)$ are the positions of the sources along the z-axis and θ is the polar angle that determines the observation direction. It must be noted that, when the array is in receiving mode, the currents I_m $(m = 1, \ldots, M)$ act as multipliers of the signals x_m $(m = 1, \ldots, M)$ created by the point sources due to the reception of DIS and N UISs. Since the use of matrix notation is more convenient for calculations in the complex frequency domain, we may consider that $I_m = w_m^*$, where w_m is a weight that expresses the conjugate value of the mth current. Then, (1) is transformed into the form

$$AF(\theta) = \sum_{m=1}^{M} w_m^* \exp(j\beta z_m \cos\theta) = \mathbf{w}^H \mathbf{a}(\theta) \tag{2}$$

where

$$\mathbf{w} = [w_1 \quad \cdots \quad w_M]^T \tag{3}$$

is the weight vector, and

$$\mathbf{a}(\theta) = [\exp(j\beta z_1 \cos\theta) \quad \cdots \quad \exp(j\beta z_M \cos\theta)]^T \tag{4}$$

is the "steering vector" that corresponds to the observation angle θ, while the superscripts T and H indicate the transpose operation and the Hermitian transpose operation, respectively.

The MVDR method aims at minimizing the mean power of the beamformer output signal component created by UISs and noise, while keeping the output signal component created by DIS undistorted [1], [2]. To achieve these goals, the weight vector must be calculated according to the expression

$$\mathbf{w}_{MV} = \frac{\mathbf{R}_{xx}^{-1}\mathbf{a}(\theta_0)}{\mathbf{a}^H(\theta_0)\mathbf{R}_{xx}^{-1}\mathbf{a}(\theta_0)} \tag{5}$$

where $\mathbf{a}(\theta_0)$ is the steering vector that corresponds to AoA θ_0 of DIS, and $\mathbf{R}_{xx}$ is the correlation matrix of the signals x_m $(m = 1, \ldots, M)$.

The MVDR method can also be applied as a DoA estimation method, that is, a method that calculates the values of AoAs of all the received signals [1], [2]. In fact, these values correspond to the local maxima of the "spatial spectrum" of the beamformer output mean power, which is given by the following formula:

$$P_{\text{out}}(\theta) = \frac{1}{\mathbf{a}^H(\theta)\mathbf{R}_{xx}^{-1}\mathbf{a}(\theta)} \tag{6}$$

where $P_{\text{out}}(\theta)$ expresses the mean power of the beamformer output signal as a function of the observation angle θ and is maximized when θ coincides with AoA of an incoming signal. It is evident from (6) that the calculation of this spectrum is based upon matrix $\mathbf{R}_{xx}$. Changes in AoAs of the incoming signals create changes in x_m $(m = 1, \ldots, M)$ and therefore changes in $\mathbf{R}_{xx}$, resulting finally in a spatial spectrum with new local maxima that correspond to the new values of AoAs θ_n $(n = 0, 1, \ldots, N)$.

The NSB method aims at nullifying the beamformer output signal component created by UISs, while keeping the output signal component created by DIS undistorted [1], [2]. To achieve these goals, the weight vector must be calculated according to the expression

$$\mathbf{w}_{NS} = \mathbf{A}(\mathbf{A}^H\mathbf{A})^{-1}\mathbf{u}_1 \tag{7}$$

where

$$\mathbf{A} = [\mathbf{a}(\theta_0) \quad \mathbf{a}(\theta_1) \quad \cdots \quad \mathbf{a}(\theta_N)] \tag{8}$$

is an $M \times (N+1)$ matrix, called as the "total steering matrix," constructed by the steering vectors that correspond to AoAs of all the received signals (i.e., DIS and N UISs), and

$$\mathbf{u}_1 = [1 \quad 0 \quad \cdots \quad 0]^T \tag{9}$$

is a unit vector composed of $N+1$ elements.

The theoretical BF model is based upon specific assumptions, which are given next.

1) There is no correlation between DIS s_0 and any UIS s_i $(i = 1, \ldots, N)$.
2) There is no correlation between any two noise signals n_i and n_j $(i, j = 1, \ldots, M)$ created at the positions of the array elements, which means that the noise correlation matrix $\mathbf{R}_{nn}$ is well approximated as

$$\mathbf{R}_{nn} = P_n \mathbf{I}_{M\times M} \tag{10}$$

where P_n is the noise mean power and $\mathbf{I}_{M\times M}$ is the $M \times M$ identity matrix.
3) There is no correlation between any incoming signal s_i $(i = 0, 1, \ldots, N)$ and any noise signal n_j $(j = 1, \ldots, M)$.

It is considered that these three assumptions apply to the realistic BF model as well. Due to these assumptions, the SINR is calculated by the following formula:

$$\text{SINR[dB]} = 10 \log \left(\frac{P_{s0}\, \mathbf{w}^H\, \mathbf{a}(\theta_0)\, \mathbf{a}^H(\theta_0)\, \mathbf{w}}{\mathbf{w}^H\, \mathbf{A}_u\, \mathbf{R}_{uu}\, \mathbf{A}_u^H\, \mathbf{w} + P_n\, \mathbf{w}^H\, \mathbf{w}} \right) \tag{11}$$

where P_{s0} is the mean power of DIS, $\mathbf{R}_{uu}$ is the correlation matrix of UISs, and

$$\mathbf{A}_u = [\mathbf{a}(\theta_1) \quad \cdots \quad \mathbf{a}(\theta_N)] \tag{12}$$

is the steering matrix of UISs ($M \times N$ matrix), also called as the "UISs steering matrix." Furthermore, due to the third assumption, $\mathbf{R}_{xx}$ can be expressed as follows:

$$\mathbf{R}_{xx} = \mathbf{A}\, \mathbf{R}_{ss}\, \mathbf{A}^H + \mathbf{R}_{nn} \tag{13}$$

where $\mathbf{R}_{ss}$ is the correlation matrix of all the received signals (i.e., DIS and N UISs). Finally, due to (10) (i.e., the second assumption), (13) is transformed into the form

$$\mathbf{R}_{xx} = \mathbf{A}\, \mathbf{R}_{ss}\, \mathbf{A}^H + P_n\, \mathbf{I}_{M\times M}. \tag{14}$$

IV. Modified BF Methods

In reality, an antenna array is not composed of ideal point sources but consists of elements, which produce a particular nonisotropic radiation pattern and interact with each other due to mutual coupling. So, let us consider an antenna array composed of M rectangular microstrip elements ($M > N$), which are parallel to the yz-plane, are arranged along the z-axis and are uniformly spaced at distance d, as shown in Fig. 1. The microstrip elements are constructed according to the inset-feeding technique [43], [44], because they can easily achieve an input impedance equal to 50 Ω without the need for any additional matching network. The input of every element is located in the middle of the element side, which is parallel to the z-axis. Consequently, the electric theta-component E_θ is negligible on the xz-plane at directions around the x-axis compared to the electric phi-component E_φ ($E_\theta \ll E_\varphi$). To validate this assumption, several trials were carried out, where E_θ and E_φ were calculated by performing a full-wave analysis on the microstrip array with the CST software package [45]. All the comparisons between E_θ and E_φ validated the above assumption at least for values of θ within the angular sector [30°, 150°]. So, the total radiation pattern of the realistic array on the xz-plane can be represented only by E_φ, which in turn is a function of angle θ.

Furthermore, E_φ can be expressed in the form

$$E_\varphi(\theta) = \sum_{m=1}^{M} I_m\, e_{\varphi m}(\theta) \tag{15}$$

where $e_{\varphi m}(\theta)$ is the electric phi-component produced by the whole array when only a unitary current is considered at the input of the mth microstrip element and all the other currents are equal to zero. It is apparent that the actual radiation pattern of the microstrip elements and the mutual coupling between them are incorporated in every $e_{\varphi m}(\theta)$. All these components $(e_{\varphi m}(\theta), m = 1, \ldots, M)$ can be extracted by performing a full-wave analysis on the microstrip array with the CST. To validate (15), several comparisons were carried out between the radiation pattern $E_\varphi(\theta)$ of the array derived directly by the CST and $E_\varphi(\theta)$ derived by (15). All the comparisons exhibited absolute similarity.

By considering that $I_m = w_m^*$ and by applying the matrix notation as in the case of the theoretical antenna array model, (15) is transformed into the form

$$E_\varphi(\theta) = \sum_{m=1}^{M} w_m^*\, e_{\varphi m}(\theta) = \mathbf{w}^H\, \mathbf{e}_\varphi(\theta) \tag{16}$$

where

$$\mathbf{e}_\varphi(\theta) = [e_{\varphi 1}(\theta) \quad \cdots \quad e_{\phi M}(\theta)]^T \tag{17}$$

is a vector constructed by all the electric phi-components $e_{\varphi m}(\theta)$ $(m = 1, \ldots, M)$ that correspond to a certain polar angle θ, and therefore it can be called as the "electric phi-vector." By comparing (2) and (16), which express the total radiation patterns of the theoretical and the realistic array, respectively, on the xz-plane, we see that they are both produced by the dot product of the weight vector $\mathbf{w}$ and another vector, which is the steering vector in the case of the theoretical array or the electric phi-vector in the case of the realistic array. In other words, if $\mathbf{a}(\theta)$ is replaced by $\mathbf{e}_\varphi(\theta)$, then a transition is made from the radiation pattern of the theoretical array to the radiation pattern of the realistic array. Furthermore, if this replacement is made in any expression that applies to the theoretical array, then the modified expression will apply to the realistic array. Such replacements are going to be made in the expressions of the MVDR and NSB methods, as given in the following.

By replacing every $\mathbf{a}(\theta_n)$ with $\mathbf{e}_\varphi(\theta_n)$ in (7) and (14), we, respectively, get

$$\mathbf{w}_{NS} = \mathbf{E}_\varphi \left(\mathbf{E}_\varphi^H \mathbf{E}_\varphi \right)^{-1} \mathbf{u}_1 \tag{18}$$

and

$$\mathbf{R}_{xx} = \mathbf{E}_{\varphi}\,\mathbf{R}_{ss}\,\mathbf{E}_{\varphi}^{H} + P_n\,\mathbf{I}_{M\times M} \tag{19}$$

where

$$\mathbf{E}_{\varphi} = [\mathbf{e}_{\varphi}(\theta_0) \quad \mathbf{e}_{\varphi}(\theta_1) \quad \cdots \quad \mathbf{e}_{\varphi}(\theta_N)] \tag{20}$$

is an $M\times(N+1)$ matrix, similar to $\mathbf{A}$ in structure, constructed by the electric phi-vectors that correspond to AoAs of all the incoming signals, and therefore it can be called as the "total electric phi-matrix." Furthermore, due to (19) and by replacing $\mathbf{a}(\theta_0)$ with $\mathbf{e}_{\varphi}(\theta_0)$ in (5), we get

$$\mathbf{w}_{MV} = \frac{\left(\mathbf{E}_{\varphi}\,\mathbf{R}_{ss}\,\mathbf{E}_{\varphi}^{H} + P_n\,\mathbf{I}_{M\times M}\right)^{-1}\mathbf{e}_{\varphi}(\theta_0)}{\mathbf{e}_{\varphi}^{H}(\theta_0)\left(\mathbf{E}_{\varphi}\,\mathbf{R}_{ss}\,\mathbf{E}_{\varphi}^{H} + P_n\,\mathbf{I}_{M\times M}\right)^{-1}\mathbf{e}_{\varphi}(\theta_0)}. \tag{21}$$

Finally, by replacing every $\mathbf{a}(\theta_n)$ with $\mathbf{e}_{\varphi}(\theta_n)$ in (11), we get

$$\text{SINR [dB]} = 10\log\left(\frac{P_{s0}\,\mathbf{w}^{H}\,\mathbf{e}_{\varphi}(\theta_0)\,\mathbf{e}_{\varphi}^{H}(\theta_0)\,\mathbf{w}}{\mathbf{w}^{H}\,\mathbf{E}_{\varphi u}\,\mathbf{R}_{uu}\,\mathbf{E}_{\varphi u}^{H}\,\mathbf{w} + P_n\,\mathbf{w}^{H}\,\mathbf{w}}\right) \tag{22}$$

where

$$\mathbf{E}_{\varphi u} = [\mathbf{e}_{\varphi}(\theta_1) \quad \cdots \quad \mathbf{e}_{\varphi}(\theta_N)] \tag{23}$$

is an $M\times N$ matrix, similar to $\mathbf{A}_u$ in structure, constructed by the electric phi-vectors that correspond to AoAs of UISs. So, $\mathbf{E}_{\varphi u}$ can be called as the "UISs electric phi-matrix." It is apparent that (18), (19), (21), and (22) apply to the realistic BF model.

What is really important is to have a beamformer capable of providing reliable results with the least possible information. A beamformer based on the NSB method needs to know only AoAs of the received signals. From these angles, the beamformer constructs $\mathbf{E}_{\varphi}$ using (20) and finally calculates the weight vector using (18). The MVDR method seems to be more demanding than the NSB method, because it needs to know the matrix $\mathbf{R}_{ss}$ besides AoAs of the received signals. Thus, it would be really noteworthy if the MVDR method could work effectively using only the values of AoAs θ_n $(n = 0, 1, \ldots, N)$ and without the knowledge of the matrix $\mathbf{R}_{ss}$, as happens with the NSB method. For this purpose, we decided to assume that $P_{sn} = 1$ $(n = 0, 1, \ldots, N)$ and also that there is no correlation between any two incoming signals. Under these two assumptions, $\mathbf{R}_{ss}$ and $\mathbf{R}_{uu}$ can be well approximated as identity matrices. Then, (21) and (22) are replaced, respectively, by the expressions

$$\mathbf{w}_{MV} = \frac{\left(\mathbf{E}_{\varphi}\mathbf{E}_{\varphi}^{H} + P_n\mathbf{I}_{M\times M}\right)^{-1}\mathbf{e}_{\varphi}(\theta_0)}{\mathbf{e}_{\varphi}^{H}(\theta_0)\left(\mathbf{E}_{\varphi}\mathbf{E}_{\varphi}^{H} + P_n\mathbf{I}_{M\times M}\right)^{-1}\mathbf{e}_{\varphi}(\theta_0)} \tag{24}$$

and

$$\text{SINR[dB]} = 10\log\left(\frac{\mathbf{w}^{H}\mathbf{e}_{\varphi}(\theta_0)\,\mathbf{e}_{\varphi}^{H}(\theta_0)\,\mathbf{w}}{\mathbf{w}^{H}\mathbf{E}_{\varphi u}\,\mathbf{E}_{\varphi u}^{H}\,\mathbf{w} + P_n\mathbf{w}^{H}\,\mathbf{w}}\right) \tag{25}$$

where P_n may be extracted from the SNR as follows:

$$P_n = 10^{-\text{SNR}/10}. \tag{26}$$

By replacing $\mathbf{a}(\theta)$ with $\mathbf{e}_{\varphi}(\theta)$ in (6), we derive the expression

$$P_{\text{out}}(\theta) = \frac{1}{\mathbf{e}_{\varphi}^{H}(\theta)\,\mathbf{R}_{xx}^{-1}\,\mathbf{e}_{\varphi}(\theta)} \tag{27}$$

which is used for DoA estimation in the realistic case. It is obvious that the only information used by (27) to perform DoA estimation is provided by $\mathbf{R}_{xx}$. Since, in our article, $\mathbf{R}_{xx}$ is not constructed from experimental data but is simulated through $\mathbf{R}_{ss}$ using (19), we must not consider $\mathbf{R}_{ss}$ as an identity matrix, because if we do so, we will lose useful information about the incoming signals and finally (27) will wrongly estimate the spatial spectrum. For good agreement with the reality, it is better to calculate $\mathbf{R}_{ss}$ from samples of the incoming signals.

V. Optimization of Realistic Microstrip Linear Array

The linear antenna array employed by the beamformer is intended for operation at 800 MHz and consists of 16 microstrip rectangular patches ($M = 16$) uniformly spaced at a fixed distance $d = \lambda/2$ (λ is the wavelength at 800 MHz). The patches are considered to be developed on a Rogers RT/duroid 5880 substrate that has a thickness $h = 1.575$ mm and an electric permittivity $\varepsilon_r = 2.2$ [46]. The thickness of the copper cladding, used in the CST for the modeling of the microstrip patches and the ground plane at both sides of the substrate, is considered to be equal to 35 μm.

In real life, an antenna array usually satisfies requirements that have a practical value, like impedance matching. Therefore, it would be of great interest to compose the array with microstrip elements matched to 50 Ω sources (like a commercial microstrip array). To do so, the microstrip elements are designed by applying the inset-feeding technique [43], [44]. This technique helps the array elements to easily achieve impedance matching. The parameters (W, L, q, g, δ, t) used to describe the microstrip geometry that implements the inset-feeding technique are shown in Fig. 1.

Since the mutual coupling between the microstrip elements affects their input impedance, the impedance matching condition can be satisfied by optimizing the whole array under a requirement for S-parameters, which is $S_{m,m} \leq -20$ dB $(m = 1, \ldots, 16)$ at the input points of the 16 microstrip elements. The optimization is performed by applying a PSO variant called "PSO with velocity mutation" (PSOvm) [47]. In fact, the PSOvm algorithm employs the CST to perform a full-wave analysis on the whole microstrip array and extract the values of $S_{m,m}$ $(m = 1, \ldots, 16)$ at the input points of the 16 microstrip elements. These values are gradually minimized through the iterative procedure of the PSOvm algorithm and finally become equal to or less than –20 dB. The optimization is performed considering that all the array elements have equal currents at their inputs (i.e., all the input currents are equal to $1 + \text{j}0$).

The optimized array geometry and the respective values of $S_{m,m}$ $(m = 1, \ldots, 16)$ at the inputs of the microstrip elements are shown in Table I. It seems that the impedance matching

TABLE I
GEOMETRY PARAMETERS AND $S_{m,m}$ VALUES OF THE OPTIMIZED ARRAY

Geometry Parameter	Value (mm)	S-parameter	Value (dB)
Under Optimization:		$S_{1,1}$ & $S_{16,16}$	–17.60
W	152.4	$S_{2,2}$ & $S_{15,15}$	–22.91
L	124.6	$S_{3,3}$ & $S_{14,14}$	–20.44
q	4.9	$S_{4,4}$ & $S_{13,13}$	–21.55
g	3.3	$S_{5,5}$ & $S_{12,12}$	–20.86
δ	39.0	$S_{6,6}$ & $S_{11,11}$	–21.32
t	4.7	$S_{7,7}$ & $S_{10,10}$	–21.03
Fixed:		$S_{8,8}$ & $S_{9,9}$	–21.17
d	187.5		
h	1.575		
ε_r	2.2		

condition is fairly approximated by the two elements at the ends of the array (1st and 16th) but is fully satisfied by the rest of the array elements ($m = 2, \ldots, 15$). Since the purpose of this article is not the optimization of the microstrip array, we decided to keep this geometry and to use it in the modified BF methods. The only information needed by this geometry to be incorporated in the modified BF methods is the electric phi-components $e_{\varphi m}(\theta)$, $m = 1, \ldots, 16$. These components are extracted for all the values of angle θ between 0° and 180° with step 0.01°, by performing a full-wave analysis on the optimized array with the CST.

VI. RESULTS

To demonstrate the validity and the effectiveness of the proposed modification, both expressions (18) and (24) are used to calculate the weight vectors in ten different scenarios of signal reception. Each scenario concerns a DIS and a predefined number N of UISs, all received by the antenna array at the same time from different DoAs. It is noted that the number N of UISs coincides with the sequential number (Nth) of the scenario. All AoAs must be chosen within the angular sector [30°, 150°], because the assumption $E_\theta \ll E_\varphi$ comes true for polar angles within this sector (as explained in the first paragraph of Section IV). To be able to extract conclusions with respect to the spatial distribution of the incoming signals, the angular distance $\Delta\theta$ between any two adjacent signals (i.e., either between any two UISs or between DIS and any UIS) is not defined at random but is considered to have a certain value, that is, 6°, 8°, or 10°. So, in every Nth scenario, a large number of combinations of $N + 1$ AoAs can be created as follows.

1) Starting from the lower boundary (30°) of the above sector, we define a set of $N + 1$ equidistant angles with an angular spacing $\Delta\theta$, that is, 30°, 30° + $\Delta\theta$, 30° + 2$\Delta\theta$, ..., 30° + $N\Delta\theta$.
2) We define $N + 1$ combinations of angles, considering, each time, a different angle from the above set as AoA θ_0 of DIS and the other angles as AoAs of UISs, that is, $\theta_0 = 30°$ in the first combination, $\theta_0 = 30° + \Delta\theta$ in the second combination, ..., $\theta_0 = 30° + N\Delta\theta$ in the $(N + 1)$th combination.
3) We increase all the angles of the previous set by a slight step, for example, 0.1°, thus creating a new set of $N+1$ equidistant angles with an angular spacing $\Delta\theta$ (that is, 30.1°, 30.1° + $\Delta\theta$, 30.1° + 2$\Delta\theta$, ..., 30.1° + $N\Delta\theta$).
4) We define additional $N + 1$ combinations of angles, considering, each time, a different angle from the above set as AoA θ_0 of DIS and the other angles as AoAs of UISs.
5) We repeat steps 3 and 4, until the biggest angle of the created set becomes greater than 150°, that is, outside the sector [30°, 150°].

TABLE II
MEAN VALUE AND STANDARD DEVIATION OF THE MAIN LOBE DIVERGENCE, THE NULLS DIVERGENCE, AND THE SINR, FOR $\Delta\theta = 6°$ AND SNR = 0 dB

	Divergence of mainlobe (deg) [mean/std]	Divergence of nulls (deg) [mean/std]	SINR (dB) [mean/std]
Scenario 1: 1 DIS – 1 UIS			
Modified MVDR algorithm	1.09/0.83	0.00/0.00	26.73/3.38
Modified NSB algorithm	1.09/0.83	0.00/0.00	26.73/3.38
Scenario 2: 1 DIS – 2 UISs			
Modified MVDR algorithm	1.25/1.11	0.01/0.03	26.26/3.81
Modified NSB algorithm	1.26/1.12	0.00/0.00	26.25/3.82
Scenario 3: 1 DIS – 3 UISs			
Modified MVDR algorithm	1.30/1.37	0.03/0.07	25.55/4.39
Modified NSB algorithm	1.32/1.40	0.00/0.00	25.52/4.44
Scenario 4: 1 DIS – 4 UISs			
Modified MVDR algorithm	1.38/1.53	0.07/0.18	24.62/5.05
Modified NSB algorithm	1.41/1.58	0.00/0.00	24.53/5.17
Scenario 5: 1 DIS – 5 UISs			
Modified MVDR algorithm	1.40/1.65	0.15/0.40	23.50/5.62
Modified NSB algorithm	1.46/1.68	0.00/0.00	23.30/5.90
Scenario 6: 1 DIS – 6 UISs			
Modified MVDR algorithm	1.40/1.73	0.25/0.59	22.24/5.99
Modified NSB algorithm	1.48/1.76	0.00/0.00	21.82/6.53
Scenario 7: 1 DIS – 7 UISs			
Modified MVDR algorithm	1.37/1.79	0.36/0.71	20.83/6.12
Modified NSB algorithm	1.49/1.83	0.00/0.00	20.07/7.02
Scenario 8: 1 DIS – 8 UISs			
Modified MVDR algorithm	1.34/1.84	0.48/0.81	19.25/6.03
Modified NSB algorithm	1.52/1.90	0.00/0.00	17.98/7.35
Scenario 9: 1 DIS – 9 UISs			
Modified MVDR algorithm	1.30/1.91	0.63/0.87	17.53/5.80
Modified NSB algorithm	1.55/2.00	0.00/0.00	15.51/7.54
Scenario 10: 1 DIS – 10 UISs			
Modified MVDR algorithm	1.25/1.99	0.84/0.93	15.74/5.56
Modified NSB algorithm	1.59/2.12	0.00/0.00	12.59/7.65

In total, all ten scenarios are implemented for two different values of SNR, that is, 0 and 10 dB, and for three different values of $\Delta\theta$, that is, 6°, 8°, and 10°. Then, a statistical analysis is performed per value of $\Delta\theta$, per value of SNR, and per scenario, thus calculating the mean values and standard deviations (std's) of 1) the divergence of the main lobe direction from DoA of DIS, 2) the direction divergence of the nulls from DoAs of the respective UISs, and 3) the SINR. The statistical results are presented in Tables II–VII.

Tables II–VII reveal a causality between the results. Looking at Tables IV–VII, we observe a slight increase in the divergence of the main lobe direction, that is, an increase of about 0.1° in the mean value and up to 0.1° in the standard deviation, and practically no divergence in the positions of the nulls, as we move from the first to the tenth scenario. The slight

TABLE III

MEAN VALUE AND STANDARD DEVIATION OF THE MAIN LOBE DIVERGENCE, THE NULLS DIVERGENCE, AND THE SINR, FOR $\Delta\theta = 6°$ AND SNR = 10 dB

	Divergence of mainlobe (deg) [mean/std]	Divergence of nulls (deg) [mean/std]	SINR (dB) [mean/std]
Scenario 1: 1 DIS – 1 UIS			
Modified MVDR algorithm	1.09/0.83	0.00/0.00	36.73/3.38
Modified NSB algorithm	1.09/0.83	0.00/0.00	36.73/3.38
Scenario 2: 1 DIS – 2 UISs			
Modified MVDR algorithm	1.26/1.12	0.00/0.00	36.25/3.82
Modified NSB algorithm	1.26/1.12	0.00/0.00	36.25/3.82
Scenario 3: 1 DIS – 3 UISs			
Modified MVDR algorithm	1.32/1.40	0.00/0.01	35.52/4.44
Modified NSB algorithm	1.32/1.40	0.00/0.00	35.52/4.44
Scenario 4: 1 DIS – 4 UISs			
Modified MVDR algorithm	1.41/1.58	0.00/0.02	34.54/5.16
Modified NSB algorithm	1.41/1.58	0.00/0.00	34.53/5.17
Scenario 5: 1 DIS – 5 UISs			
Modified MVDR algorithm	1.45/1.69	0.01/0.05	33.32/5.87
Modified NSB algorithm	1.46/1.68	0.00/0.00	33.30/5.90
Scenario 6: 1 DIS – 6 UISs			
Modified MVDR algorithm	1.47/1.77	0.03/0.11	31.88/6.46
Modified NSB algorithm	1.48/1.76	0.00/0.00	31.82/6.53
Scenario 7: 1 DIS – 7 UISs			
Modified MVDR algorithm	1.48/1.86	0.07/0.21	30.18/6.88
Modified NSB algorithm	1.49/1.83	0.00/0.00	30.07/7.02
Scenario 8: 1 DIS – 8 UISs			
Modified MVDR algorithm	1.50/1.95	0.12/0.33	28.21/7.09
Modified NSB algorithm	1.52/1.90	0.00/0.00	27.98/7.35
Scenario 9: 1 DIS – 9 UISs			
Modified MVDR algorithm	1.51/2.06	0.19/0.45	25.94/7.11
Modified NSB algorithm	1.55/2.00	0.00/0.00	25.51/7.54
Scenario 10: 1 DIS – 10 UISs			
Modified MVDR algorithm	1.51/2.20	0.29/0.57	23.39/6.98
Modified NSB algorithm	1.59/2.12	0.00/0.00	22.59/7.65

TABLE IV

MEAN VALUE AND STANDARD DEVIATION OF THE MAIN LOBE DIVERGENCE, THE NULLS DIVERGENCE, AND THE SINR, FOR $\Delta\theta = 8°$ AND SNR = 0 dB

	Divergence of mainlobe (deg) [mean/std]	Divergence of nulls (deg) [mean/std]	SINR (dB) [mean/std]
Scenario 1: 1 DIS – 1 UIS			
Modified MVDR algorithm	0.50/0.46	0.00/0.00	27.31/2.92
Modified NSB algorithm	0.50/0.46	0.00/0.00	27.31/2.92
Scenario 2: 1 DIS – 2 UISs			
Modified MVDR algorithm	0.53/0.43	0.00/0.00	27.60/2.76
Modified NSB algorithm	0.53/0.43	0.00/0.00	27.60/2.76
Scenario 3: 1 DIS – 3 UISs			
Modified MVDR algorithm	0.52/0.43	0.00/0.01	27.85/2.65
Modified NSB algorithm	0.53/0.43	0.00/0.00	27.85/2.65
Scenario 4: 1 DIS – 4 UISs			
Modified MVDR algorithm	0.52/0.44	0.00/0.01	28.04/2.58
Modified NSB algorithm	0.52/0.44	0.00/0.00	28.04/2.59
Scenario 5: 1 DIS – 5 UISs			
Modified MVDR algorithm	0.51/0.45	0.00/0.02	28.18/2.54
Modified NSB algorithm	0.52/0.45	0.00/0.00	28.17/2.54
Scenario 6: 1 DIS – 6 UISs			
Modified MVDR algorithm	0.51/0.46	0.00/0.02	28.24/2.52
Modified NSB algorithm	0.51/0.46	0.00/0.00	28.24/2.52
Scenario 7: 1 DIS – 7 UISs			
Modified MVDR algorithm	0.52/0.46	0.00/0.02	28.25/2.51
Modified NSB algorithm	0.52/0.46	0.00/0.00	28.25/2.51
Scenario 8: 1 DIS – 8 UISs			
Modified MVDR algorithm	0.54/0.46	0.01/0.02	28.19/2.52
Modified NSB algorithm	0.54/0.46	0.00/0.00	28.19/2.52
Scenario 9: 1 DIS – 9 UISs			
Modified MVDR algorithm	0.57/0.46	0.01/0.03	28.07/2.55
Modified NSB algorithm	0.58/0.47	0.00/0.00	28.06/2.55
Scenario 10: 1 DIS – 10 UISs			
Modified MVDR algorithm	0.63/0.47	0.01/0.03	27.88/2.61
Modified NSB algorithm	0.63/0.47	0.00/0.00	27.87/2.61

increase in the divergence of the main lobe direction can be explained by the fact that the increase in the number of UISs creates difficulty in finding DoA of DIS. However, both the modified methods demonstrate a remarkable accuracy in the positions of the nulls, regardless of the number of UISs or the SNR value. This is because null steering is the first priority task for both the methods.

A comparison between Tables IV and V or between Tables VI and VII shows that the SNR does not affect the divergence of the main lobe. Also, the mean values and standard deviations of the SINR are almost the same in Tables IV and VI, where SNR $= 0$ dB, while an increase by 10 dB is observed in the SINR values in Tables V and VII, where SNR $= 10$ dB. As we move from Table IV or V (where $\Delta\theta = 8°$) to Table VI or VII (where $\Delta\theta = 10°$), respectively, we observe a slight decrease of about $0.1°$ in the mean value of the main lobe divergence and practically no change in the standard deviation of the main lobe divergence. This slight decrease is due to the increase in $\Delta\theta$, which makes the closest nulls at both sides of the main lobe move away from the main lobe peak and therefore the main lobe has less difficulty in finding DoA of DIS.

The main lobe half-width of every antenna array has a lower boundary, which depends on the array geometry (i.e., the distances between the array elements and the element type). This boundary, expressed as $\Delta\theta_{\min}$, is the minimum possible distance between the main lobe peak and a null, and is the actual parameter that affects the ability of the beamformer to steer not only the main lobe toward DoA of DIS but also the nulls toward DoAs of the respective UISs. When $\Delta\theta$ is greater than $\Delta\theta_{\min}$, the main lobe fits more easily between any two consecutive nulls and can therefore be steered toward DoA of DIS with better accuracy, while the nulls are steered exactly toward DoAs of the respective UISs, and all these take place regardless of the value of the SNR as previously mentioned. All these happen for $\Delta\theta = 8°$ and even more for $\Delta\theta = 10°$.

On the contrary, when $\Delta\theta = 6°$ (see Tables II and III), the beamformer is forced to put at least a null very close to the main lobe peak, that is, at a distance less than $\Delta\theta_{\min}$. Therefore, either the main lobe peak or a null or both will diverge from their respective preassigned directions. For this reason, the mean value and standard deviation of the main lobe divergence are greater than the respective values derived for the same SNR and for $\Delta\theta = 8°$ or $10°$.

By comparing the results of the modified NSB algorithm derived for $\Delta\theta = 6°$ and for any scenario, we observe no change in any divergence value (either mean value or standard deviation of either the main lobe or the nulls) when increasing the SNR from 0 (Table II) to 10 dB (Table III). This can be explained by the fact that (18) does not take into account the SNR to calculate the weight vector. The zero divergence of the nulls is due to the fact that null steering is the first priority

TABLE V

MEAN VALUE AND STANDARD DEVIATION OF THE MAIN LOBE DIVERGENCE, THE NULLS DIVERGENCE, AND THE SINR, FOR $\Delta\theta = 8°$ AND SNR = 10 dB

	Divergence of mainlobe (deg) [mean/std]	Divergence of nulls (deg) [mean/std]	SINR (dB) [mean/std]
Scenario 1: 1 DIS – 1 UIS			
Modified MVDR algorithm	0.50/0.46	0.00/0.00	37.31/2.92
Modified NSB algorithm	0.50/0.46	0.00/0.00	37.31/2.92
Scenario 2: 1 DIS – 2 UISs			
Modified MVDR algorithm	0.53/0.43	0.00/0.00	37.60/2.76
Modified NSB algorithm	0.53/0.43	0.00/0.00	37.60/2.76
Scenario 3: 1 DIS – 3 UISs			
Modified MVDR algorithm	0.53/0.43	0.00/0.00	37.85/2.65
Modified NSB algorithm	0.53/0.43	0.00/0.00	37.85/2.65
Scenario 4: 1 DIS – 4 UISs			
Modified MVDR algorithm	0.52/0.44	0.00/0.00	38.04/2.59
Modified NSB algorithm	0.52/0.44	0.00/0.00	38.04/2.59
Scenario 5: 1 DIS – 5 UISs			
Modified MVDR algorithm	0.51/0.45	0.00/0.00	38.17/2.54
Modified NSB algorithm	0.52/0.45	0.00/0.00	38.17/2.54
Scenario 6: 1 DIS – 6 UISs			
Modified MVDR algorithm	0.51/0.46	0.00/0.00	38.24/2.52
Modified NSB algorithm	0.51/0.46	0.00/0.00	38.24/2.52
Scenario 7: 1 DIS – 7 UISs			
Modified MVDR algorithm	0.52/0.46	0.00/0.00	38.25/2.51
Modified NSB algorithm	0.52/0.46	0.00/0.00	38.25/2.51
Scenario 8: 1 DIS – 8 UISs			
Modified MVDR algorithm	0.54/0.46	0.00/0.00	38.19/2.52
Modified NSB algorithm	0.54/0.46	0.00/0.00	38.19/2.52
Scenario 9: 1 DIS – 9 UISs			
Modified MVDR algorithm	0.58/0.47	0.00/0.00	38.06/2.55
Modified NSB algorithm	0.58/0.47	0.00/0.00	38.06/2.55
Scenario 10: 1 DIS – 10 UISs			
Modified MVDR algorithm	0.63/0.47	0.00/0.00	37.87/2.61
Modified NSB algorithm	0.63/0.47	0.00/0.00	37.87/2.61

TABLE VI

MEAN VALUE AND STANDARD DEVIATION OF THE MAIN LOBE DIVERGENCE, THE NULLS DIVERGENCE, AND THE SINR, FOR $\Delta\theta = 10°$ AND SNR = 0 dB

	Divergence of mainlobe (deg) [mean/std]	Divergence of nulls (deg) [mean/std]	SINR (dB) [mean/std]
Scenario 1: 1 DIS – 1 UIS			
Modified MVDR algorithm	0.45/0.42	0.00/0.00	27.34/2.70
Modified NSB algorithm	0.45/0.42	0.00/0.00	27.34/2.70
Scenario 2: 1 DIS – 2 UISs			
Modified MVDR algorithm	0.43/0.44	0.00/0.02	27.65/2.49
Modified NSB algorithm	0.43/0.44	0.00/0.00	27.65/2.49
Scenario 3: 1 DIS – 3 UISs			
Modified MVDR algorithm	0.40/0.43	0.00/0.02	27.88/2.38
Modified NSB algorithm	0.40/0.43	0.00/0.00	27.88/2.38
Scenario 4: 1 DIS – 4 UISs			
Modified MVDR algorithm	0.38/0.41	0.00/0.02	28.03/2.32
Modified NSB algorithm	0.38/0.41	0.00/0.00	28.03/2.32
Scenario 5: 1 DIS – 5 UISs			
Modified MVDR algorithm	0.37/0.41	0.00/0.02	28.09/2.29
Modified NSB algorithm	0.37/0.41	0.00/0.00	28.09/2.29
Scenario 6: 1 DIS – 6 UISs			
Modified MVDR algorithm	0.37/0.41	0.00/0.02	28.06/2.29
Modified NSB algorithm	0.37/0.41	0.00/0.00	28.06/2.29
Scenario 7: 1 DIS – 7 UISs			
Modified MVDR algorithm	0.39/0.41	0.00/0.02	27.95/2.30
Modified NSB algorithm	0.39/0.42	0.00/0.00	27.95/2.30
Scenario 8: 1 DIS – 8 UISs			
Modified MVDR algorithm	0.42/0.44	0.00/0.02	27.75/2.35
Modified NSB algorithm	0.42/0.44	0.00/0.00	27.75/2.35
Scenario 9: 1 DIS – 9 UISs			
Modified MVDR algorithm	0.48/0.48	0.00/0.02	27.45/2.46
Modified NSB algorithm	0.48/0.48	0.00/0.00	27.44/2.46
Scenario 10: 1 DIS – 10 UISs			
Modified MVDR algorithm	0.54/0.53	0.00/0.02	27.05/2.66
Modified NSB algorithm	0.54/0.53	0.00/0.00	27.05/2.66

task for the NSB algorithm. So, if the distance between a null and the main lobe peak is less than $\Delta\theta_{\min}$, then consequences may exist only for the main lobe steering.

Contrary to the NSB, the modified MVDR algorithm makes use of noise information to calculate the weight vector as shown in (24). In particular, the noise mean power P_n is added to the elements of the main diagonal of the matrix $\mathbf{E}_\varphi \mathbf{E}_\varphi^H$ before the matrix is inverted according to (24). This process is similar to the diagonal loading technique used in singular or ill-conditioned matrices prior to their inversion. In this way, the matrix inversion performed in (24) is always possible. However, the value of P_n affects the accuracy of the result. If P_n has a low value (when the SNR is high), the elements of the main diagonal of the matrix $\mathbf{E}_\varphi \mathbf{E}_\varphi^H$ are not significantly modified and therefore the nulls are placed to the right directions, that is, with low divergence. This behavior is observed in Table III where SNR = 10 dB, is similar to that of the modified NSB algorithm, and is explained in the same way (i.e., because null steering is the first priority task for both the methods). Due to this behavior, divergence is induced only in the main lobe steering for both the methods. On the contrary, if P_n is high (when the SNR is low), the elements of the main diagonal of the matrix $\mathbf{E}_\varphi \mathbf{E}_\varphi^H$ are significantly modified, and this creates difficulty in placing the nulls to the right directions, meaning that a divergence is induced in the directions of the nulls. This is observed in Table II where SNR = 0 dB. Nevertheless, the existence of divergence in the directions of the nulls decreases the difficulty in steering the main lobe to the right direction, thus reducing the main lobe divergence. We could say that the increased value of P_n helps the modified MVDR algorithm to create a balance between the main lobe divergence and the divergence of the nulls.

As shown in Tables II and III, the main lobe divergence and the divergence of the nulls affect the SINR, which is dramatically reduced with increasing the number of UISs. Therefore, when $\Delta\theta$ is less than $\Delta\theta_{\min}$ (i.e., when $\Delta\theta = 6°$), the only way to reduce the main lobe divergence together with the divergence of the nulls is to increase the number of elements that compose the antenna array. This can be explained by the fact that an increase in the number of array elements causes a decrease in $\Delta\theta_{\min}$ (because the main lobe becomes narrower). In this way, $\Delta\theta$ becomes greater than $\Delta\theta_{\min}$, and therefore the main lobe peak and a null can come very close to each other without diverging from their respective preassigned directions.

To have a perception of the radiation patterns produced by the modified BF methods, four typical patterns of the tenth scenario (1 DIS and 10 UISs) produced by the two methods for SNR equal to 0 and 10 dB and for $\Delta\theta$ equal to 10° are shown in Figs. 2–5. Deep drops in the directional gain are observed at DoAs of UISs, while the peak of the main lobe is steered exactly toward DoA of DIS. This accuracy in the

TABLE VII

MEAN VALUE AND STANDARD DEVIATION OF THE MAIN LOBE DIVERGENCE, THE NULLS DIVERGENCE, AND THE SINR, FOR $\Delta\theta = 10°$ AND SNR = 10 dB

	Divergence of mainlobe (deg) [mean/std]	Divergence of nulls (deg) [mean/std]	SINR (dB) [mean/std]
Scenario 1: 1 DIS – 1 UIS			
Modified MVDR algorithm	0.45/0.42	0.00/0.00	37.34/2.70
Modified NSB algorithm	0.45/0.42	0.00/0.00	37.34/2.70
Scenario 2: 1 DIS – 2 UISs			
Modified MVDR algorithm	0.43/0.44	0.00/0.00	37.65/2.49
Modified NSB algorithm	0.43/0.44	0.00/0.00	37.65/2.49
Scenario 3: 1 DIS – 3 UISs			
Modified MVDR algorithm	0.40/0.43	0.00/0.00	37.88/2.38
Modified NSB algorithm	0.40/0.43	0.00/0.00	37.88/2.38
Scenario 4: 1 DIS – 4 UISs			
Modified MVDR algorithm	0.38/0.41	0.00/0.00	38.03/2.32
Modified NSB algorithm	0.38/0.41	0.00/0.00	38.03/2.32
Scenario 5: 1 DIS – 5 UISs			
Modified MVDR algorithm	0.37/0.41	0.00/0.00	38.09/2.29
Modified NSB algorithm	0.37/0.41	0.00/0.00	38.09/2.29
Scenario 6: 1 DIS – 6 UISs			
Modified MVDR algorithm	0.37/0.41	0.00/0.00	38.06/2.29
Modified NSB algorithm	0.37/0.41	0.00/0.00	38.06/2.29
Scenario 7: 1 DIS – 7 UISs			
Modified MVDR algorithm	0.39/0.42	0.00/0.00	37.95/2.30
Modified NSB algorithm	0.39/0.42	0.00/0.00	37.95/2.30
Scenario 8: 1 DIS – 8 UISs			
Modified MVDR algorithm	0.42/0.44	0.00/0.00	37.75/2.35
Modified NSB algorithm	0.42/0.44	0.00/0.00	37.75/2.35
Scenario 9: 1 DIS – 9 UISs			
Modified MVDR algorithm	0.48/0.48	0.00/0.00	37.44/2.46
Modified NSB algorithm	0.48/0.48	0.00/0.00	37.44/2.46
Scenario 10: 1 DIS – 10 UISs			
Modified MVDR algorithm	0.54/0.53	0.00/0.00	37.05/2.66
Modified NSB algorithm	0.54/0.53	0.00/0.00	37.05/2.66

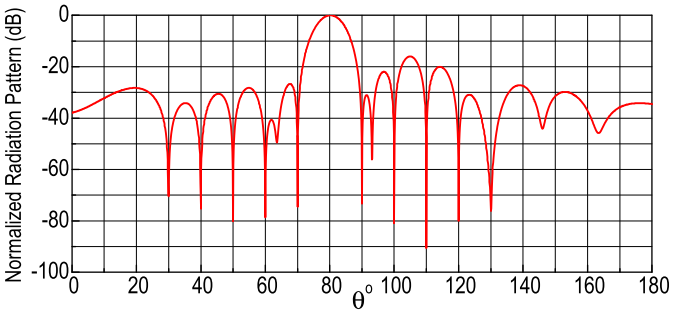

Fig. 2. Radiation pattern produced by the modified MVDR algorithm for a case of the tenth scenario with $\Delta\theta = 10°$, where a DIS is received at 80° and 10 UISs are received at respective angles equal to 30°, 40°, 50°, 60°, 70°, 90°, 100°, 110°, 120°, and 130°, in the presence of noise with SNR = 0 dB.

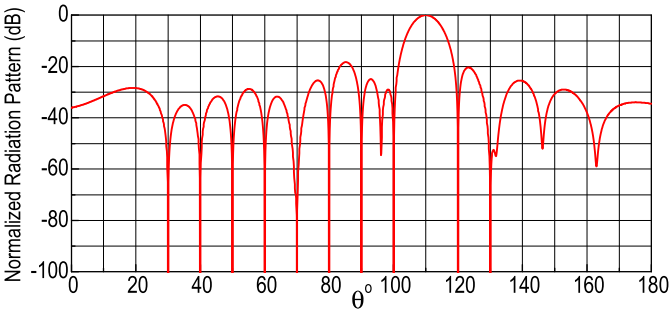

Fig. 3. Radiation pattern produced by the modified NSB algorithm for a case of the tenth scenario with $\Delta\theta = 10°$, where a DIS is received at 110° and 10 UISs are received at respective angles equal to 30°, 40°, 50°, 60°, 70°, 80°, 90°, 100°, 120°, and 130°, in the presence of noise with SNR = 0 dB.

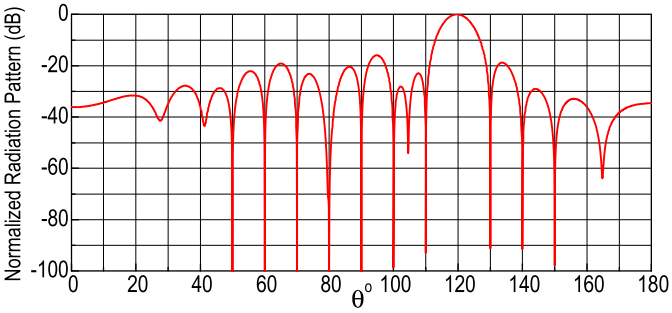

Fig. 4. Radiation pattern produced by the modified MVDR algorithm for a case of the tenth scenario with $\Delta\theta = 10°$, where a DIS is received at 120° and 10 UISs are received at respective angles equal to 50°, 60°, 70°, 80°, 90°, 100°, 110°, 130°, 140°, and 150°, in the presence of noise with SNR = 10 dB.

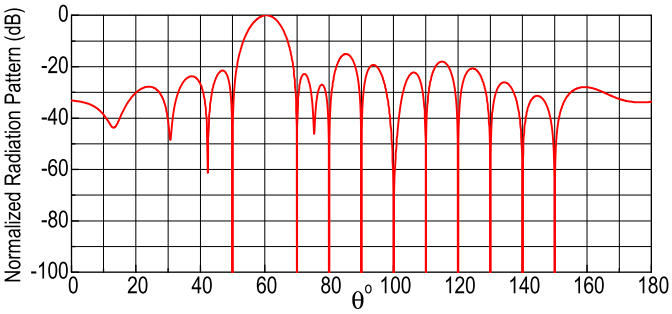

Fig. 5. Radiation pattern produced by the modified NSB algorithm for a case of the tenth scenario with $\Delta\theta = 10°$, where a DIS is received at 60° and 10 UISs are received at respective angles equal to 50°, 70°, 80°, 90°, 100°, 110°, 120°, 130°, 140°, and 150°, in the presence of noise with SNR = 10 dB.

positions of the nulls and the position of the main lobe is verified by the statistical results of Tables VI and VII.

The validity and effectiveness of the proposed modification are also examined, when the modified BF methods are applied in combination with a DoA estimation algorithm modified in a similar way to incorporate realistic conditions that take place in an antenna array. Such conditions have already been considered in (27), which expresses the spatial spectrum produced by the MVDR-based DoA estimation algorithm in the case of a realistic antenna array model. The previously described ten scenarios are repeated in the same way for two different values of SNR, that is, 0 and 10 dB. For every incoming signal, 100 simulated samples are produced by a random number generator function following a normal distribution with a mean of 0 and a standard deviation of 1 (the standard deviation of the samples of an incoming signal is expressed by $\sqrt{P_{sn}}$, while $P_{sn} = 1$, where $n = 0, 1, \ldots, N$). These samples are utilized to create the matrix $\mathbf{R}_{ss}$, which is used in (19) to construct the matrix $\mathbf{R}_{xx}$, which in turn is used in (27) to estimate the values of AoAs of the incoming signals. Then, the values of AoAs are sent as an input to the modified BF methods, which in turn calculate the weight vector using (18) or (24). The statistical analysis performed per value of SNR and per scenario, in the same way as before, shows that the involvement of the DoA

estimation algorithm does not perceptibly affect the efficiency of the modified BF methods.

VII. Conclusion

By applying a proper modification as proposed in this article, the particular nonisotropic radiation pattern produced by the specific element type used to compose the antenna array and the mutual coupling between the array elements can be incorporated as information into conventional beamformers, making them capable of working effectively in practice, that is, when the beamformers are applied to realistic antenna arrays. In this way, the above modification brings the BF algorithms closer to real-life applications. The thorough statistical analysis performed on the modified versions of the MVDR and NSB algorithms reveals that the algorithms have an excellent ability to create nulls extremely close to DoAs of respective UISs as well as a main lobe very close to DoA of DIS, and all these regardless of the noise level, but provided that the angular distance between the main lobe peak and a null does not become less than a lower boundary, which depends on the geometry of the antenna array employed by the beamformer. An additional statistical analysis shows that the involvement of an MVDR-based DoA estimation algorithm properly modified for the realistic model does not perceptibly downgrade the efficiency of the modified BF methods. The modified beamformers are able to work effectively when using not only microstrip linear arrays but also any type of antenna array, provided that characteristic electric field components, like those ($e_{\varphi m}$) used in this article, will be given as information to the beamformers.

References

[1] L. Godara, *Smart Antennas*. Boca Raton, FL, USA: CRC Press, 2004.

[2] F. B. Gross, *Smart Antennas for Wireless Communications With MATLAB*. New York, NY, USA: McGraw-Hill, 2005.

[3] J. Li and P. Stoica, *Robust Adaptive Beamforming*. Hoboken, NJ, USA: Wiley, 2006.

[4] C. A. Olen and R. T. Compton, "A numerical pattern synthesis algorithm for arrays," *IEEE Trans. Antennas Propag.*, vol. 38, no. 10, pp. 1666–1676, Oct. 1990.

[5] C. C. Chai and Y. C. Liang, "Joint MIMO beamforming and power adaptation at base station and broadcasting relay transmitters with quality-of-service (QoS) constraints," in *Proc. IEEE Veh. Technol. Conf. (VTC Spring)*, May 2008, pp. 1026–1031.

[6] J. Park and S. Lee, "MIMO beamforming for QoS enhancement via analog, digital and hybrid relaying," *IEEE Trans. Broadcast.*, vol. 56, no. 4, pp. 494–503, Dec. 2010.

[7] M. Lertsutthiwong, T. Nguyen, and B. Hamdaoui, "Efficient wireless broadcasting through joint network coding and beamforming," *Int. J. Digit. Multimedia Broadcast.*, vol. 2012, Mar. 2012, Art. no. 342512.

[8] J. Park and S. Lee, "M2-m2 beamforming for virtual MIMO broadcasting in multi-hop relay networks," *IEEE J. Sel. Areas Commun.*, vol. 30, no. 8, pp. 1358–1369, Sep. 2012.

[9] P. Kasemir, N. Sutton, M. Radway, B. Jeong, T. Brown, and D. S. Filipovic, "Wideband analog and digital beamforming," in *Proc. 9th Int. Conf. Telecommun. Mod. Satell., Cable, Broadcast. Services*, Niš, Serbia, Oct. 2009, pp. 372–375.

[10] J. A. Srar, K.-S. Chung, and A. Mansour, "Adaptive array beamforming using a combined LMS-LMS algorithm," *IEEE Trans. Antennas Propag.*, vol. 58, no. 11, pp. 3545–3557, Nov. 2010.

[11] L. Zhang, W. Liu, and R. J. Langley, "Adaptive beamforming with real-valued coefficients based on uniform linear arrays," *IEEE Trans. Antennas Propag.*, vol. 59, no. 3, pp. 1047–1053, Mar. 2011.

[12] F. Liu, J. Wang, C. Y. Sun, and R. Du, "Robust MVDR beamformer for nulling level control via multi-parametric quadratic programming," *Prog. Electromagn. Res. C*, vol. 20, pp. 239–254, 2011.

[13] K. Yang, Z. Zhao, X. Zhu, and Q. H. Liu, "Robust adaptive beamforming with low sidelobe levels," in *Proc. IEEE Antennas Propag. Soc. Int. Symp. (APSURSI)*, Orlando, FL, USA, Jul. 2013, pp. 872–873.

[14] Y. Yang, L. Yang, and J. Zhu, "Sidelobe suppression for time-domain adaptive broadband beamforming with sparse constraint," in *Proc. MTS/IEEE Monterey OCEANS*, Monterey, CA, USA, Sep. 2016, pp. 1–4.

[15] M. A. Sarker, M. S. Hossain, and M. S. Masud, "Robust beamforming synthesis technique for low side lobe level using Taylor excited antenna array," in *Proc. 2nd Int. Conf. Electr., Comput. Telecommun. Eng. (ICECTE)*, Rajshahi, Bangladesh, Dec. 2016, pp. 1–4.

[16] I. P. Gravas, Z. D. Zaharis, T. V. Yioultsis, P. I. Lazaridis, and T. D. Xenos, "Adaptive beamforming with sidelobe suppression by placing extra radiation pattern nulls," *IEEE Trans. Antennas Propag.*, vol. 67, no. 6, pp. 3853–3862, Jun. 2019.

[17] G. Gottardi, L. Poli, P. Rocca, A. Montanari, A. Aprile, and A. Massa, "Optimal monopulse beamforming for side-looking airborne radars," *IEEE Antennas Wireless Propag. Lett.*, vol. 16, pp. 1221–1224, 2017.

[18] G. Gottardi, N. Ebrahimi, P. Rocca, and A. Massa, "Optimal synthesis of monopulse beamforming weights for airborne radars through convex optimization," in *Proc. Int. Appl. Comput. Electromagn. Soc. Symp. (ACES)*, Firenze, Italy, Mar. 2017, pp. 1–2.

[19] Y. Liu, X. Huang, K. D. Xu, Z. Song, S. Yang, and Q. H. Liu, "Pattern synthesis of unequally spaced linear arrays including mutual coupling using iterative FFT via virtual active element pattern expansion," *IEEE Trans. Antennas Propag.*, vol. 65, no. 8, pp. 3950–3958, Aug. 2017.

[20] M. M. Roshanaei, C. Lucas, and A. R. Mehrabian, "Adaptive beamforming using a novel numerical optimisation algorithm," *IET Microw., Antennas Propag.*, vol. 3, no. 5, pp. 765–773, Aug. 2009.

[21] Z. D. Zaharis and T. V. Yioultsis, "A novel adaptive beamforming technique applied on linear antenna arrays using adaptive mutated Boolean PSO," *Prog. Electromagn. Res.*, vol. 117, pp. 165–179, 2011.

[22] R. Mallipeddi, J. P. Lie, P. N. Suganthan, S. G. Razul, and C. M. S. See, "A differential evolution approach for robust adaptive beamforming based on joint estimation of look direction and array geometry," *Prog. Electromagn. Res.*, vol. 119, pp. 381–394, 2011.

[23] L. Poli, P. Rocca, G. Oliveri, and A. Massa, "Harmonic beamforming in time-modulated linear arrays," *IEEE Trans. Antennas Propag.*, vol. 59, no. 7, pp. 2538–2545, Jul. 2011.

[24] Z. D. Zaharis, C. Skeberis, and T. D. Xenos, "Improved antenna array adaptive beamforming with low side lobe level using a novel adaptive invasive weed optimization method," *Prog. Electromagn. Res.*, vol. 124, pp. 137–150, 2012.

[25] S. Jayaprakasam, S. K. B. A. Rahim, and C. Y. Leow, "A Pareto elite selection genetic algorithm for random antenna array beamforming with low sidelobe level," *Prog. Electromagn. Res. B*, vol. 51, pp. 407–425, 2013.

[26] N. Anselmi, P. Rocca, A. Massa, and E. Giaccari, "Synthesis of robust beamforming weights in linear antenna arrays," in *Proc. IEEE Conf. Antenna Meas. Appl. (CAMA)*, Antibes Juan-les-Pins, France, Nov. 2014, pp. 1–3.

[27] N. Anselmi, P. Rocca, M. Salucci, and A. Massa, "Optimisation of excitation tolerances for robust beamforming in linear arrays," *IET Microw., Antennas Propag.*, vol. 10, no. 2, pp. 208–214, Jan. 2016.

[28] S. E. El-Khamy, A. S. Eltrass, and H. F. El-Sayed, "Design of thinned fractal antenna arrays for adaptive beam forming and sidelobe reduction," *IET Microw., Antennas Propag.*, vol. 12, no. 3, pp. 435–441, Feb. 2018.

[29] A. H. E. Zooghby, C. G. Christodoulou, and M. Georgiopoulos, "Neural network-based adaptive beamforming for one- and two-dimensional antenna arrays," *IEEE Trans. Antennas Propag.*, vol. 46, no. 12, pp. 1891–1893, Dec. 1998.

[30] X. Song, J. Wang, and X. Niu, "Robust adaptive beamforming algorithm based on neural network," in *Proc. IEEE Int. Conf. Automat. Logistics*, Qingdao, China, Sep. 2008, pp. 1844–1849.

[31] Z. D. Zaharis, K. A. Gotsis, and J. N. Sahalos, "Adaptive beamforming with low side lobe level using neural networks trained by mutated Boolean PSO," *Prog. Electromagn. Res.*, vol. 127, pp. 139–154, 2012.

[32] Z. D. Zaharis, C. Skeberis, T. D. Xenos, P. I. Lazaridis, and J. Cosmas, "Design of a novel antenna array beamformer using neural networks trained by modified adaptive dispersion invasive weed optimization based data," *IEEE Trans. Broadcast.*, vol. 59, no. 3, pp. 455–460, Sep. 2013.

[33] P. Mousavi, M. Fakharzadeh, and S. Safavi-Naeini, "1K element antenna system for mobile direct broadcasting satellite reception," *IEEE Trans. Broadcast.*, vol. 56, no. 3, pp. 340–349, Sep. 2010.
[34] N. A. Sutton and D. S. Filipovic, "V-band monolithically integrated four-arm spiral antenna and beamforming network," in *Proc. IEEE Int. Symp. Antennas Propag.*, Chicago, IL, USA, Jul. 2012, pp. 1–2.
[35] L. Yang, G. Ren, W. Zhai, and Z. Qiu, "Beamforming based receiver scheme for DVB-T2 system in high speed train environment," *IEEE Trans. Broadcast.*, vol. 59, no. 1, pp. 146–154, Mar. 2013.
[36] A. Young, M. V. Ivashina, R. Maaskant, O. A. Iupikov, and D. B. Davidson, "Improving the calibration efficiency of an array fed reflector antenna through constrained beamforming," *IEEE Trans. Antennas Propag.*, vol. 61, no. 7, pp. 3538–3545, Jul. 2013.
[37] D. S. Prinsloo, M. V. Ivashina, R. Maaskant, and P. Meyer, "Beamforming strategies for active multi-mode antennas: Maximum gain, signal-to-noise ratio, and polarization discrimination," in *Proc. Int. Conf. Electromagn. Adv. Appl. (ICEAA)*, Palm Beach, Aruba, Aug. 2014, pp. 507–510.
[38] O. Jo *et al.*, "Holistic design considerations for environmentally adaptive 60 GHz beamforming technology," *IEEE Commun. Mag.*, vol. 52, no. 11, pp. 30–38, Nov. 2014.
[39] O. A. Iupikov *et al.*, "An optimal beamforming algorithm for phased-array antennas used in multi-beam spaceborne radiometers," in *Proc. 9th Eur. Conf. Antennas Propag.*, Lisbon, Portugal, Aug. 2015, pp. 1–5.
[40] O. A. Iupikov, M. V. Ivashina, C. Cappellin, and N. Skou, "Digital-beamforming array antenna technologies for future ocean-observing satellite missions," in *Proc. IEEE Int. Symp. Antennas Propag. (APSURSI)*, Fajardo, Puerto Rico, Jun. 2016, pp. 1377–1378.
[41] O. A. Iupikov, M. V. Ivashina, N. Skou, C. Cappellin, K. Pontoppidan, and C. G. M. van Klooster, "Multibeam focal plane arrays with digital beamforming for high precision space-borne ocean remote sensing," *IEEE Trans. Antennas Propag.*, vol. 66, no. 2, pp. 737–748, Feb. 2018.
[42] O. Manoochehri, D. Erricolo, A. Darvazehban, and F. Monticone, "Design of compact beam-steering active slot antennas with a metasurface reflector," in *Proc. United States Nat. Committee URSI Nat. Radio Sci. Meeting (USNC-URSI NRSM)*, Boulder, CO, USA, Jan. 2019, pp. 1–2.
[43] Y. Hu, D. R. Jackson, J. T. Williams, S. A. Long, and V. R. Komanduri, "Characterization of the input impedance of the inset-fed rectangular microstrip antenna," *IEEE Trans. Antennas Propag.*, vol. 56, no. 10, pp. 3314–3318, Oct. 2008.
[44] C. Mbinack, B. Bodo, J.-S. A. E. Fouda, and E. Tonye, "Inset-fed rectangular MICROSTRIP patch antenna bandwidth enhancement," *Microw. Opt. Technol. Lett.*, vol. 61, no. 2, pp. 562–567, Feb. 2019.
[45] *CST Studio Suite*. Accessed: Oct. 16, 2019. [Online]. Available: https://www.3ds.com/products-services/simulia/products/cst-studio-suite/
[46] *Rogers Corporation*. Accessed: Oct. 16, 2019. [Online]. Available: https://www.rogerscorp.com/
[47] Z. D. Zaharis, I. P. Gravas, P. I. Lazaridis, I. A. Glover, C. S. Antonopoulos, and T. D. Xenos, "Optimal LTE-protected LPDA design for DVB-T reception using particle swarm optimization with velocity mutation," *IEEE Trans. Antennas Propag.*, vol. 66, no. 8, pp. 3926–3935, Aug. 2018.

Zaharias D. Zaharis (Senior Member, IEEE) received the B.Sc. degree in physics, the M.Sc. degree in electronics, the Ph.D. degree in antennas and propagation modeling for mobile communications, and the Diploma degree in electrical and computer engineering from the Aristotle University of Thessaloniki, Thessaloniki, Greece, in 1987, 1994, 2000, and 2011, respectively.

From 2002 to 2013, he was with the Administration of the Telecommunications Network, Aristotle University of Thessaloniki. Since 2013, he has been with the Department of Electrical and Computer Engineering, Aristotle University of Thessaloniki. His current research interests include design and optimization of antennas and microwave circuits, signal processing on smart antennas, development of evolutionary optimization algorithms, and neural networks.

Dr. Zaharis is a member of the Technical Chamber of Greece. He is currently serving as an Associate Editor for IEEE ACCESS.

Ioannis P. Gravas (Student Member, IEEE) received the Diploma degree in electrical and computer engineering from the Aristotle University of Thessaloniki, Thessaloniki, Greece, in 2017, where he is currently pursuing the Ph.D. degree. The subject of his doctoral dissertation is radiation shaping techniques for antenna arrays.

His research interests include beamforming and direction of arrival estimation techniques, design and optimization of antennas, microwave engineering, and optimization algorithms.

Pavlos I. Lazaridis (Senior Member, IEEE) received the B.Sc. degree in electrical engineering from the Aristotle University of Thessaloniki, Thessaloniki, Greece, in 1990, the M.Sc. degree in electronics from Université Pierre and Marie Curie, Paris, France, in 1992, and the Ph.D. degree from Ecole Nationale Supérieure des Télécommunications (ENST) Paris, Paris, in 1996.

From 1991 to 1996, he was involved with research for France Télécom, Paris, France, and teaching at ENST Paris. In 1997, he became the Head of the Antennas and Propagation Laboratory, Télédiffusion de France/France Télécom Research Center (TDF-C2R Metz). From 1998 to 2002, he was a Senior Examiner with the European Patent Office (EPO), The Hague, The Netherlands. From 2002 to 2014 he was involved with teaching and research with the Alexander Technological Educational Institute (ATEI) of Thessaloniki, and Brunel University, London, U.K. He is currently a Professor of electronic and electrical engineering with the University of Huddersfield, Huddersfield, U.K. He is a member of the Institution of Engineering and Technology (IET) and a fellow of the Higher Education Academy.

Traianos V. Yioultsis (Member, IEEE) received the Diploma and Ph.D. degrees in electrical and computer engineering from the Aristotle University of Thessaloniki, Thessaloniki, Greece, in 1992 and 1998, respectively.

From 2001 to 2002, he was a Post-Doctoral Research Associate with the Department of Electrical and Computer Engineering, University of Illinois at Urbana–Champaign, Champaign, IL, USA. Since 2002, he has been with the Department of Electrical and Computer Engineering, Aristotle University of Thessaloniki, where he is currently a Professor. His current interests include the analysis and design of antennas and microwave circuits with fast computational techniques, and the modeling of complex wave propagation problems.

Dr. Yioultsis has served as a member of the Editorial Board for the IEEE COMMUNICATIONS LETTERS and several international conferences.

Christos S. Antonopoulos (Senior Member, IEEE) was born in Alexandroupolis, Greece.

His major topic is numerical methods in electromagnetics, but his scientific interests also include problems dealing with electromagnetic compatibility, antennas, metamaterials, and acoustic propagation. He is currently a Professor with the Department of Electrical and Computer Engineering, Faculty of Technology, Aristotle University of Thessaloniki, Thessaloniki, Greece.

Thomas D. Xenos was born in Thessaloniki, Greece. He received the Diploma degree in electrical engineering from the University of Patras, Patras, Greece, in 1978, and the Ph.D. degree in wireless communications from the Aristotle University of Thessaloniki, Thessaloniki, in 1991.

Then, he joined the Department of Electrical and Computer Engineering, Aristotle University of Thessaloniki, where he is currently a Professor. He has participated in many national and international projects. He has authored over 85 scientific articles. His research interests include wireless communications, radio-wave propagation, nonionizing electromagnetic radiation measurements, and electromagnetic compatibility.